CONTRIBUTION TO THE DYNAMICS OF THE THREE-DIMENSIONAL FLOWS IN SQUARE-SECTIONED CURVED DUCTS

Farid GACI[1], Zoubir NEMOUCHI[1], Lyes KHEZZAR[2]

[1] Laboratoire d'Energétique Appliquée et de Pollution, Université Constantine « 1 », Algérie
[2] Mechanical Engineering Department, Petroleum Institute, Abu Dhabi, UAE.

Reçu le 03 Mai 2011 – Accepté le 15 Avril 2013

Résumé

Une étude numérique des écoulements laminaires et turbulents d'un fluide traversant des coudes *à* 90° et 180° de sections carrées a été entreprise. Un maillage tridimensionnel de cellules hexaédriques a été généré. Le schéma QUICK a été utilisé pour discrétiser le terme convectif dans les équations de transport. L'algorithme SIMPLE a été adopté pour traiter le couplage vitesse-pression. La structure de l'écoulement obtenu a présentée des caractéristiques intéressantes telles que les zones de recirculation et les paires de cellules contrarotatives.

La performance des trois différents modèles de turbulence a été évaluée: le modèle standard k-ε, le modèle k-ω SST et le modèle des contraintes de Reynolds (RSM). Dans l'ensemble, on a constaté que le modèle à plusieurs équations a donné de meilleurs résultats que les deux autres modèles d'équations. En fait, l'existence de quatre paires de cellules contrarotatives, dans la conduite droite en amont du coude, a été captée uniquement par le modèle de turbulence (RSM). En outre, la zone de recirculation le long de la paroi interne dans la deuxième partie de la courbure en U est mieux capturée par le modèle (RSM).

L'analyse des résultats a conduit à une meilleure compréhension des écoulements secondaires tridimensionnels induits et des comportements du coefficient de pression local et du coefficient de frottement.

***Mots clés** : Coude, cellules contrarotatives, écoulement secondaire, laminaire, turbulent.*

Abstract

A numerical study of laminar and turbulent fluid flows in 90° and 180° bends of square section was carried out. Three-dimensional meshes, based on hexahedral cells, were generated. The QUICK scheme was employed to discretize the convective term in the transport equations. The SIMPLE algorithm was adopted to treat the velocity-pressure coupling. The flow structure obtained showed interesting features such as recirculation zones and counter-rotating pairs of vortices.

The performance of three different turbulence models was evaluated: the standard *k-ε* model, the SST k-ω model and the Reynolds Stress Model (RSM). Overall, it was found that, the multi-equation model performed better than the two equation models. In fact, the existence of four pairs of counter rotating cells, in the straight duct upstream of the bend, were predicted by the RSM closure but not by the standard eddy viscosity model nor the SST k-ω model. Furthermore, the recirculation zone along the inner wall in the second part of the U-bend is better captured by the RSM.

The analysis of the results led to a better understanding of the induced three dimensional secondary flows and the behaviour of the local pressure coefficient and the friction coefficient.

***Keywords:** Curved duct, counter-rotating cells, secondary flow, laminar, turbulent.*

ملخص

أجريت دراسة عددية على الانسياب ألصفائحي والمضطرب للسوائل عبر الأنابيب المنحنية بـ 90 درجة و 180 درجة و ذات مقاطع مربعة. تم إنشاء شبكة خلايا سداسية الأبعاد وطبق مخطط QUICK لتفريد طرف الحمل الحراري في معادلات النقل واعتمدت خوارزمية SIMPLE لتحليل الربط بين الضغط و السرعة. لقد أظهر هيكل تدفق السوائل ميزات مثيرة للاهتمام مثل أزواج من خلايا متعاكسة الدوران.

عند تقييم أداء ثلاثة نماذج اضطراب السوائل مختلفة (نموذج *k-ε* ،نموذج SST k-ω ونموذج RSM) ، تبين بأن النموذج الأخير له أداء أفضل من النماذج الأخرى بحيث انه اظهر وجود أربعة أزواج من خلايا متعاكسة الدوران في القناة المستقيمة للأنبوب المنحني °90 بخلاف النموذجين الآخرين كما رصد منطقة إعادة دوران الخلايا على طول الجدار الداخلي في الجزء الثاني من الأنبوب المنحني °180 .

إضافة إلى ذلك، أدى تحليل النتائج إلى فهم أفضل للانسيابات الثانوية الثلاثية الأبعاد وسلوك معامل الضغط المحلي ومعامل الاحتكاك.

***الكلمات المفتاحية :** انبون منحني، خلايا متعاكسة الدوران، انسياب ثانوي، صفائحي ، مضطرب.*

Flows in curved ducts have attracted much interest amongst many researchers and engineers owing to their relevant fundamental aspects and industrial applications such as enhancing the heat transfer in piping systems and reducing losses in compressors and turbines.

Several experiments have been conducted in bends of square cross-section, with short and long straight ducts upstream of the curved portion. A particular interest is focused on the effect of flow development state on the evolution of the secondary flow motion. Pioneering works in this area were carried out by Humphrey et al. [1, 2]. Sudo et al. [3] developed an experimental investigation on the turbulent flow in a 90° circular-sectioned bend. Longitudinal, radial and circumferential mean velocity and turbulent fluctuations were obtained using the technique of the hot wire, for a Reynolds number equal to 6.10^4. The velocity field of the secondary flow, and Reynolds stress distributions in different sections of the elbow were discussed. Sudo et al. [4] conducted an experimental study of steady turbulent flow in a bend of square cross-section, for a Reynolds number equal to 4.10^4 and a curvature ratio of 4.

Numerical studies have also been reported, e.g. Cheng and Farokhi [5]. Further experimental and numerical works could be found in Humphrey et al. [2] and Chung et al. [6]. Rowe [7], Cheah et al [8] and Azzola and Humphrey [9] reported the occurrence of secondary flows, for the Reynolds numbers of 0.236 10^5, 10^5 and 1.1 10^5, generated locally near the 90° angle. They measured the mean and fluctuating velocities using the Laser Doppler Anemometry. A numerical analysis was developed by Sugiyama and Hitomi [10] for a three-dimensional turbulent flow in a 180° bend, using the Algebraic Reynolds Stress Model (ARSM).

The results are compared with experimental data. The location of the maximum streamwise velocity, which appears near the top or bottom wall in the bent tube, is predicted correctly by this model. Kim et al [11] presented an analysis of turbulent flow and heat transfer at the wall outlet to a 90° square-sectioned bend. They studied particularly the influence of secondary flow, vorticity and boundary conditions on heat transfer. Sudo et al [12] showed that the high velocity region is located in the 90° angle of the 180° bend and results from the secondary flow and the turbulence level present in this area. Bubolz et al [13] showed the effect of Dean vortices on the flow of helical and curved tubular membranes. Chung et al [14] showed that the flow separation that occurs at the exit of the bend for a low Reynolds number can cause an oscillatory flow downstream. They showed that these oscillations affect significantly the laminar convective heat transfer. Duque and Lucini [15] analyzed the development of a single phase flow of water through a 180° curved duct of variable cross-section profiles. They conclude that since the pressure drop is affected by the fluid velocity, it determines the direction and the movement of the flow in the duct. The secondary flow is generated from the high pressure region to the low pressure region. This flow dissipates after the fluid leaves the bend.

Computational fluid dynamics (CFD) will probably not replace physical experiments completely but it can significantly reduce the amount of experimental work and has motivated researchers to understand, in detail, the physical mechanisms of turbulent flow through curved ducts.

The purpose of this paper is to provide a further insight on laminar and turbulent flows through square-sectioned 90° and 180° bends. The computed results are compared with the available experimental measurements of Humphrey et al. [1,2] for laminar and turbulent flows through 90° bends and Cheah et al [8] for turbulent flows through a 180° bend using the standard k-ε model, the SST k-ω model and the Reynolds Stress Model (RSM).

1. MATHEMATICAL MODEL AND NUMERICAL RESOLUTION

1.1. Governing equations

The three dimensional, steady, laminar and turbulent flows of an incompressible constant-property fluid are described by the following continuity and momentum equations.

1.1.1. Laminar flow

$$\frac{\partial U_j}{\partial x_j} = 0 \tag{1}$$

$$\rho U_j \frac{\partial U_i}{\partial x_j} = -\frac{\partial P}{\partial x_i} + \mu \frac{\partial^2 U_i}{\partial x_j^2} \tag{2}$$

1.1.2. Turbulent flow

$$\frac{\partial \overline{U}_j}{\partial x_j} = 0 \tag{3}$$

$$\rho \ \overline{U}_j \frac{\partial}{\partial x_j}(\overline{U}_i) = -\frac{\partial \overline{P}}{\partial x_i} + \mu \frac{\partial^2 \overline{U}_i}{\partial x_j^2} + \frac{\partial}{\partial x_j}(-\rho \overline{u_i' u_j'}) \tag{4}$$

Three models are used in the present work to take into account the turbulence effects, namely the standard k-ε model [16], the SST k-ω model [17] and the seven-equation Reynolds stress model [18].

1.2. Numerical details

The computations were performed for the two flow regimes using the Fluent code [19] based on the finite-volume approach. The central differencing scheme was used to discretize the diffusion term and the QUICK scheme [20] was employed to treat the convective terms in the various transport equations.

The standard interpolation approach was employed to compute values of pressure on the faces. The coupling between the velocity components and pressure was treated using the iterative correction procedure SIMPLE [21].

1.3. Problem description

The geometries considered are similar to those used by Humphrey et al [1, 2] concerning the 90° bend of square cross-section for both laminar and turbulent flows and Cheah et al [8] concerning the 180° curved duct with square cross-section. The geometrical details are illustrated in figure 1. The fluid considered is air with density ρ = 1.225 kg/m^3 and kinematic viscosity v=1.46x10^{-5}m^2/s. The Reynolds number based on the hydraulic diameter is Re = 790 in the laminar case and Re = 4.10^4, 10^5 for the 90° and 180° curved ducts, respectively, in the turbulent case.

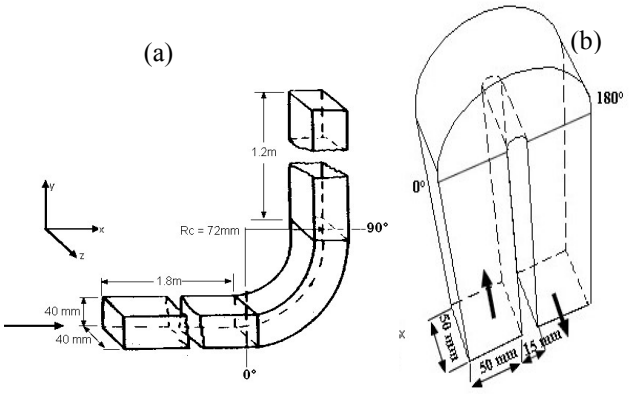

Figure 1 : Configurations : (a) 90° bend, (b) 180° bend

The boundary conditions considered are as follows.

- ***The inlet***

  - Laminar flow case:
    U: uniform profile, $V = W = 0$,

  - Turbulent flow case:
    For the 90° bend, U : uniform profile, $V = W = 0$,
    For the 180° bend, V : uniform profile, $U = W = 0$,

    ❖ Standard k- ε model and SST k-ω model:
    - Turbulent Intensity : I = 5 %
    - Hydraulic diameter : D_h = 0.04 m (90°) ,
      D_h = 0.05 m (180°)

    k and ε or ω are deduced from the prescribed turbulence intensity and the hydraulic diameter :

$$k = \frac{3}{2}(IU_b)^2 \ , \ \varepsilon = C_\mu^{3/4}\frac{k^{3/2}}{0.07D_h} \ , \ \omega = \frac{k^{1/2}}{C_\mu^{1/4}0.07D_h} \qquad (5)$$

    ❖ Reynolds Stress Model:
    Isotropic turbulence is assumed at inlet,

$$\overline{u_i' u_j'} = (2k/3)\delta_{ij}. \qquad (6)$$

- ***The outlet***

At the outlet, it is made sure that the mass flow rate leaving the domain is equal to that at the inlet. At the same time, it is assumed that a fully developed flow is attained, i.e. longitudinal gradients of the dependant variables are nil.

- ***The wall***

The no-slip condition is imposed for both laminar and turbulent flows.

In the turbulent flow case, the standard law of the wall is used.

$$U^* = \frac{1}{\kappa}\ln(Ey^*), \text{ where } U^* = \frac{U_p c_\mu^{1/4} k_p^{1/2}}{\tau_\omega/\rho} \text{ and } y^* = \frac{\rho c_\mu^{1/4} k_p^{1/2} y_p}{\mu} \qquad (7)$$

❖ When the standard k- ε or the SST k- ω models are used

$\frac{\partial k}{\partial n} = 0$, where n is the direction normal to the wall.

$\varepsilon_p = \frac{k_p^{3/2}}{C_\mu^{-3/4}\kappa y_p}$ or $\omega_p = \frac{k_p^{1/2}}{C_\mu^{1/4}\kappa y_p}$ within the cells adjacent to the wall.

❖ When the Reynolds Stress Model is used, the code computes explicitly the Reynolds stresses near the wall from :

$$\frac{\overline{u_{\tau\tau}'^2}}{k} = 1.098 \ , \ \frac{\overline{u_\eta'^2}}{k} = 0.247, \frac{\overline{u_\lambda'^2}}{k} = 0.655 \ , \ -\frac{\overline{u_\tau' u_\eta'}}{k} = 0.255 \qquad (8)$$

Close to the wall, k is obtained from its transport equation. Far from the walls k is directly obtained according to the equation:

$k = \frac{1}{2}\overline{u_i'^2}$ and ε is calculated near the wall from :

$$\varepsilon_p = \frac{k_p^{3/2}}{C_\mu^{-3/4}\kappa y_p} \qquad (9)$$

1.4. Mesh generation

The three-dimensional geometries are meshed with elementary hexahedral volumes, figure 2.

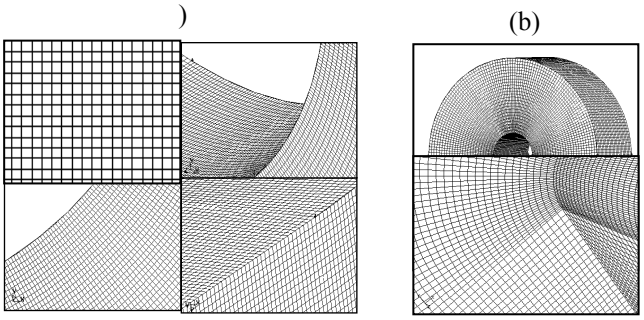

Figure 2 : Meshes considered: a) the 90° bend, b) the 180° bend

One constraint of the grid generation, when the standard wall function is employed, is the position of the centre of the first elementary volume closest to the wall.

A criterion y^+ is usually defined to characterize this cell centre location in wall coordinate, $y^+ = \frac{\rho u_\tau y}{\mu}$. It has to be greater than about 30. Where u_τ is the friction velocity, y the normal distance from the wall to the centre of the cell. In the present work, the values of y^+ range from 30 to 65.

2. RESULTS AND DISCUSSION

2.1. Laminar flow

In the present study we are concerned with manifestations of secondary flows developing in 90° and 180° bends of square cross-section connected to straight ducts upstream and downstream of the bend. This configuration allows the study of the possible appearance and persistence of coherent vortices in the domain from the inlet upstream to the outlet of the bend. The influence of the grid on the results was investigated by comparing the streamwise velocity in the 90° position of the bend. The solutions obtained are independent of the numerical mesh when 431000 and 431200 cells are used for the 90° and the 180° curved ducts respectively.

2.1.1. 90° bend

The distributions of the calculated streamwise velocities for a 90° bend configuration are plotted against the measured ones [1] at various mid-plane locations along the duct, figure 3. The velocities are normalized with respect to the inlet velocity. The results indicate a good quantitative agreement with the measurements. At the inlet plane of the bend (section of 0° angle), the fluid is slightly accelerated near the inner wall in accordance with the initially favourable longitudinal pressure gradient prevailing there, see below, figure 4. At the same time, the fluid near the outer wall is decelerated as a result of the initially adverse pressure gradient. A slight deceleration is discerned between the inlet of the bend and the 30° position along the inner wall.

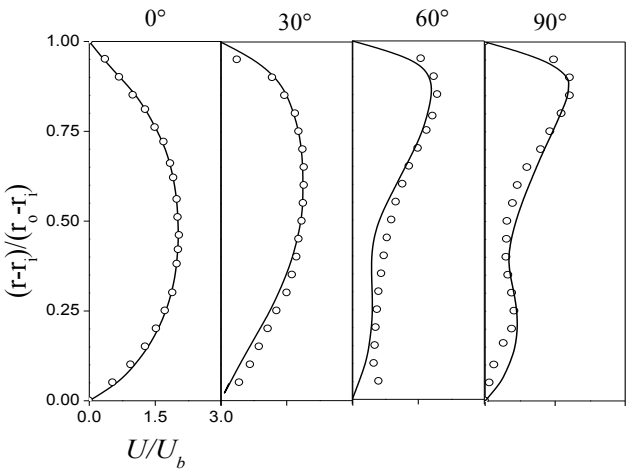

Figure 3 : Mean streamwise velocity profiles in bend

At the 30° section, the secondary flow due to the radial non equilibrium between centrifugal forces and pressure forces appears in the cross section and it forms two counter-rotating vortices wherein fluid particles circulate outward in the central part of the pipe and inward near the left and right side walls; see also figure 3. The longitudinal velocity is still relatively high near the inner wall of the bend, as before. An appreciable discrepancy between the numerical and measured data is observed near the 60° section of the duct. At the 60° section, the faster fluid near the inner wall is transported by the secondary flow towards the outer wall through the central region of the cross sections. At the 90° section, a maximum value of the velocity is reached (U/U_b = 1.78). It should be noted that numerical results obtained by Humphrey and al [1] gave a value of U/U_b = 1.61.

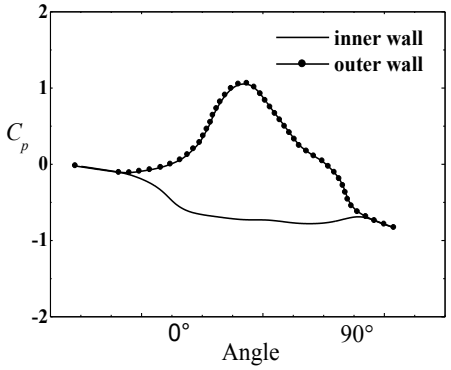

Figure 4 : Pressure coefficients along the inner and outer walls in the mid-plane

Figure 4 shows the variation of the pressure coefficient C_p inside the bend, along the inner and outer walls, versus the angle along the bend. The results reveal an important increase in pressure, i.e. adverse pressure gradient, along the outer wall at first, followed by a decrease in pressure from an angle of about 40°. On the other hand, a slight favourable pressure gradient is observed along the inner wall in the vicinity of the bend inlet. This behaviour is consistent with the obtained velocity field discussed above.

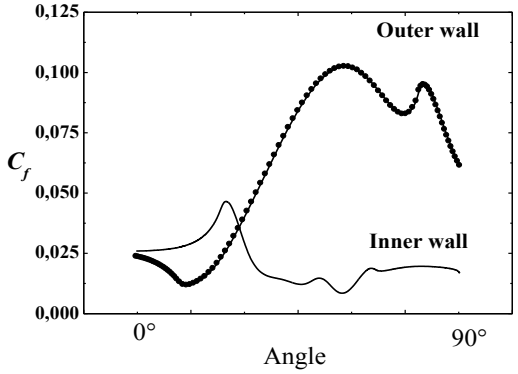

Figure 5 : Friction coefficients along the inner and outer walls in the mid-plane

The behaviour of the friction coefficient is different on the inner and outer walls, figure 5. Along the inner wall, the acceleration followed by a deceleration results in an increase in C_f followed by a decrease as this parameter

depends directly on the velocity gradient of the fluid adjacent to the wall. On the contrary, along the outer wall, the friction coefficient decreases at first indicating a tendency to separation. It then increases to a maximum value of about 0.1.

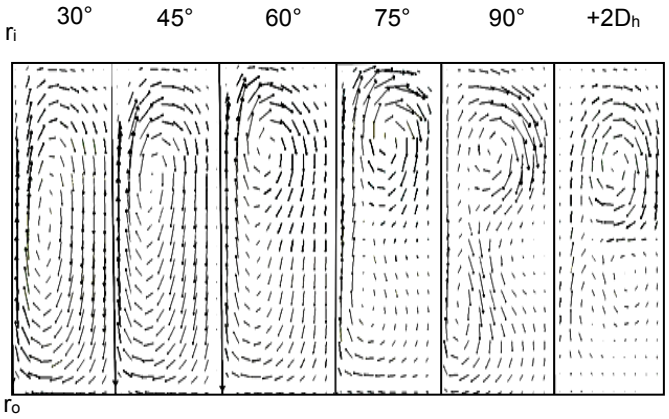

Figure 6 : Projected velocity vectors at different cross-sections of bend

Figure 6 shows the projected velocity vectors at the angles 30°, 45°, 60°, 75°, 90° and at the section 2 D_h downstream of the bend. The secondary flow displaces the fluid with relatively low streamwise momentum from the region along the side walls towards the inner-radius wall. At the same time, the fluid with high streamwise momentum from the central region is displaced along the symmetry plane toward the outer wall. The consequence of such a destabilization of the fluid layers in the bend is the birth of the Dean vortices at an angle of about 30° downstream of the inlet as illustrated by an iso-surface of the vorticity magnitude in figure 7.

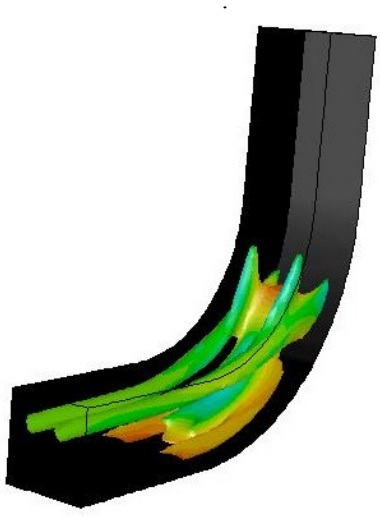

Figure 7 : Isosurface of vorticity magnitude

It is clearly seen that the cross-stream secondary vortex pair, which occupies initially the whole cross-sectional area, shifts towards the inner wall as the flow develops through the bend. This is confirmed by the position of the centre of the vortex, which is gradually displaced towards the inner radius. It is also worth noting the birth of an additional pair of counter rotating cells just underneath the primary cells and probably due to the intensity of the latter ones.

2.1.2. 180° curved duct

Figure 8 shows the variations of the pressure coefficient and the friction coefficient, along the downstream tangents of the inner and outer walls. It can be seen that within a distance of 1 D_h immediately downstream of the bend, the two curves of the pressure coefficient come together, marking the end of the bend effect on the pressure behaviour on the convex or suction side and the concave side.

Concerning the friction coefficient, however, the difference in behaviour seems to persist farther downstream. The values of C_f along the outer wall remain higher than those along the inner wall up to 2 D_h downstream of the bend where the two curves intersect (equal values of C_f on the opposite walls). Beyond that position, the values of C_f along the downstream tangent of the inner wall increase slightly higher than those along the opposite wall due to the shifting of the fluid mass towards the inner side.

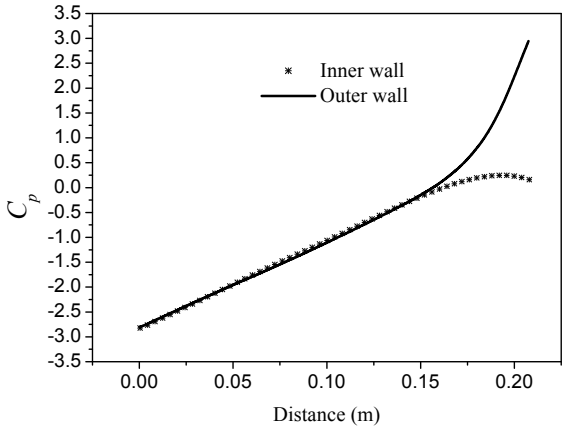

(a) Pressure coefficient

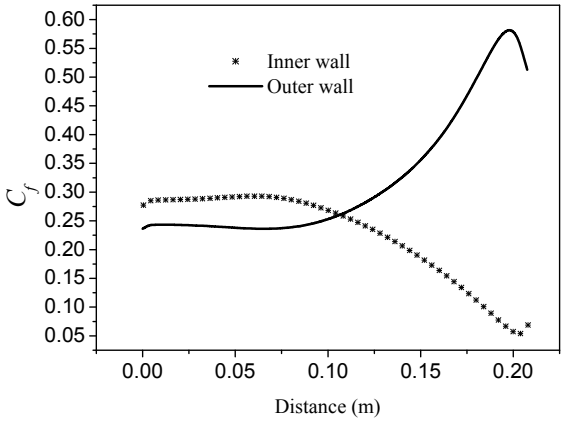

(b) Friction coefficient

Figure 8 : Pressure and friction coefficients along downstream tangents of inner and outer walls in mid-plane

Figure 9 shows streamlines, highlighting the secondary flow that prevails at the 180° angle of the bend and at 1 D_h and 2 D_h downstream of the bend. The centres of the counter rotating vortices shift from the side walls towards the symmetry plane.

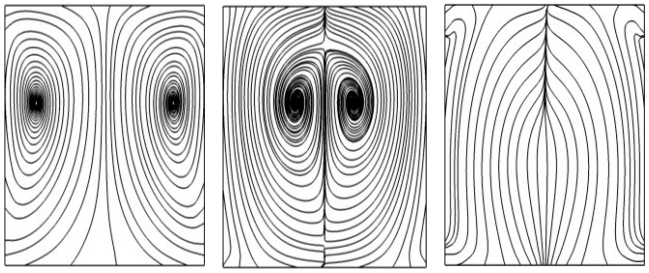

180° $+1D_h$ $+2D_h$

Figure 9 : Streamlines downstream of U-bend

The evolution of the vortex structures is clearly illustrated by the vorticity magnitude iso-surface coloured by velocity magnitude shown in figure 10. It should be noted that the flow has not fully developed yet at 2 D_h downstream of the bend.

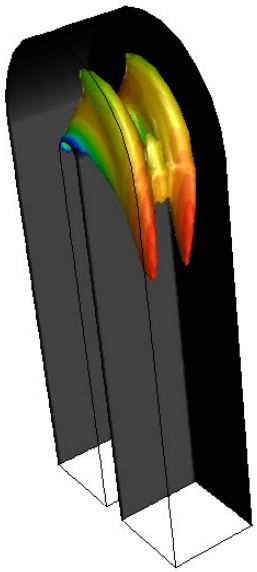

Figure 10 : Iso-surface of vorticity magnitude

2.2. Turbulent flowminar flow

2.2.1. 90° bend

The contours of the Reynolds shear stress $(\overline{u_r' u_\theta'}/U_b^2)$ at the angle 0° are illustrated in figure 11.

The numerical results of this work are in agreement with the experimental data and the RSM could capture qualitatively the general trend and the orders of magnitude.

This comparison confirms the satisfactory performance of the numerical tool employed in predicting the turbulent flow through curved ducts with the square cross-section.

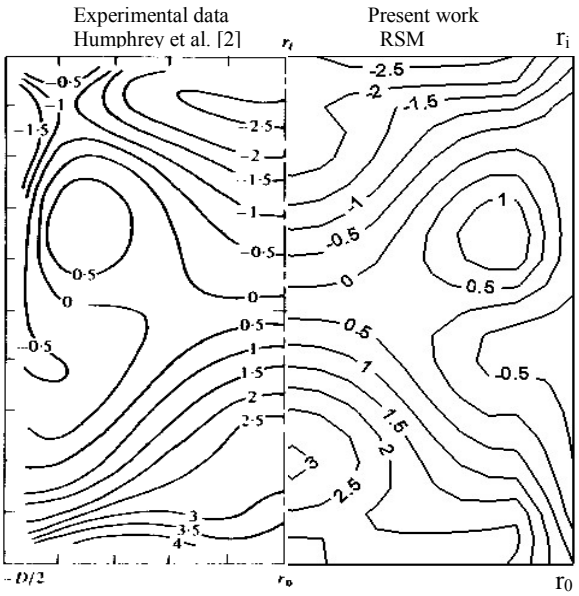

Figure 11 : Contours of $(\overline{u_r' u_\theta'}/U_b^2).10^3$ (Angle 0°)

Figure 12 shows the variations of the pressure and friction coefficients along the inner and outer walls in the mid-plane.

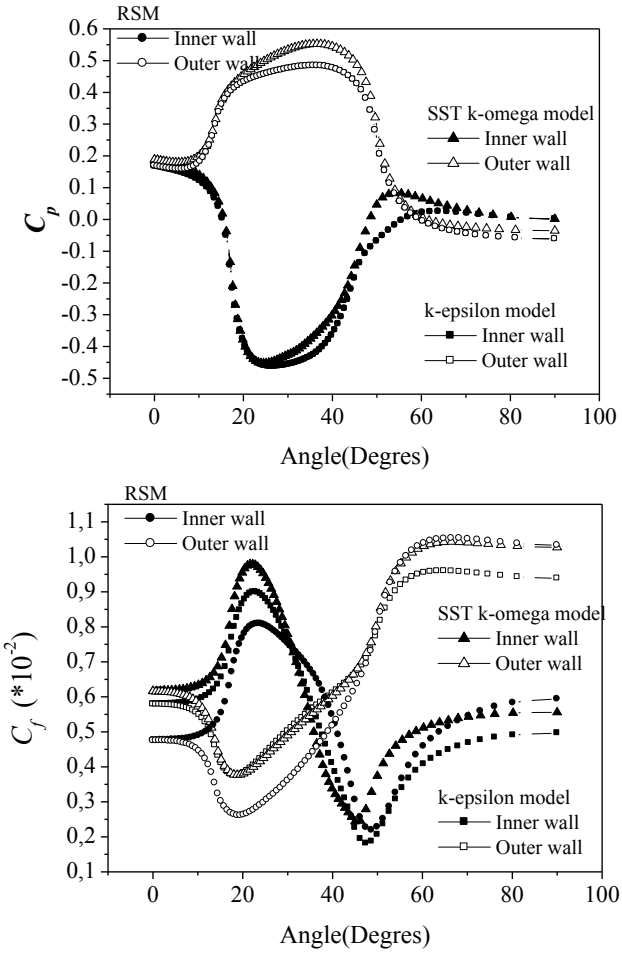

Figure 12 : Pressure and friction coefficients along the inner and outer walls in the mid-plane.

All three models predict a sharp decrease (increase) in C_p along the inner (outer) wall to a minimum (maximum) value attained at 25° (35°) position. Furthermore, the k-ε model and the SST k-ω model yield very similar extreme values ($C_{p(min)}$ = -0.45 on inner wall, $C_{p(max)}$ = 0.54 on outer wall). On the other hand, the RSM takes slightly different extreme values ($C_{p(min)}$ = -0.465 on inner wall, $C_{p(max)}$ = 0.48 on outer wall). All models predict the fact that the pressure coefficient values along the inner wall overtake those along the outer wall at the angle about 55° as obtained by the two-equation models and at 58° as obtained by the RSM.

Concerning the variation of friction coefficient, the three models predict a sharp increase along the inner wall to a maximum value of about 0.009 attained at an angle of 23° followed by a decrease to a minimum value of about 0.002. Along the outer wall, the minimum value of C_f (0.0026), reached at the angle of 20°, obtained by the RSM, is significantly smaller than that obtained by the other two models (0.0038). The friction coefficient as calculated by the three models, then increases rapidly to a maximum value of 0.010 attained at the angle of 64°. When using the standard k-ε and the SST k-ω models the C_f values along the outer wall surpass those along the inner wall at the angle of 35° while the RSM yields a point of intersection of the two curves at the angle of 40°. It is very important to note the appreciable difference in behaviour simulated at the inlet of the bend by the RSM compared to the two other models. In effect, the relatively smaller values of C_f obtained by the RSM along the mid-plane in the vicinity of the bend inlet are explained by the existence of the four pairs of the counter-rotating vortices that could not be detected by the k-ε and the SST k-ω models, as illustrated in figure 13.

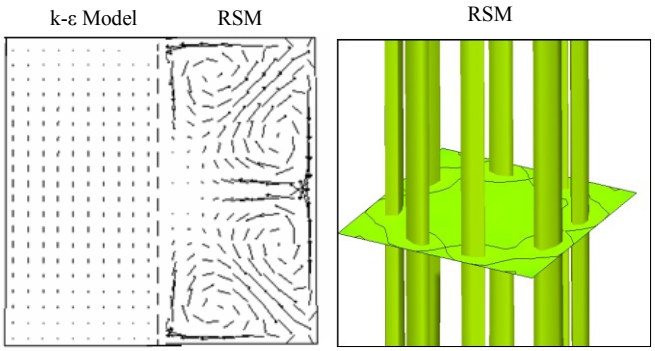

Figure 13 : Projected velocity vectors and vorticity magnitude iso-surface at position 2.5D_h upstream of the bend.

Indeed, this figure shows clearly such behaviour at 2.5 D_h upstream of the bend using an iso-surface of the vorticity magnitude and projected velocity vectors. In fact, these result in a decrease in velocity gradient and hence in C_f obtained by the RSM along the middle lines of the walls and an intensification of C_f on either side of these lines.

Figure 14 portrays the projected streamlines at three sections within the bend, at the angles 45°, 71° and 90° using the three turbulence models. At the 45° position, the four pairs of counter-rotating vortices detected by the RSM have completely disappeared.

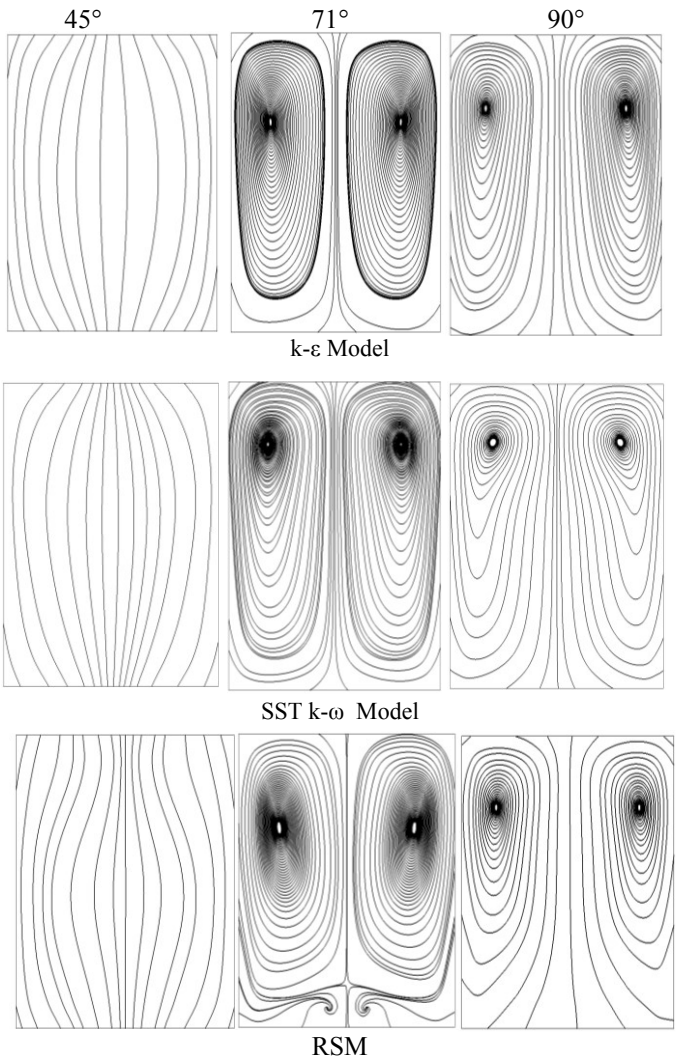

Figure 14 : Projected streamlines at different angles within the bend.

At the angles of 71° and 90°, we observe that the core of the Dean vortices as predicted by the SST k-ω model is relatively close to the inner wall compared to the other models. A weak secondary pair of counter-rotating vortices obtained using the RSM appears at the angle of 71° along the outer wall.

2.2.2. 180° curved duct

The geometry considered, a 180° square-section bend, studied experimentally by Cheah et al [8], is similar to that of an internal cooling passage of a turbine blade. Figure 15 compares streamwise mean velocity profiles predicted using the three turbulent models considered, with experimental data reported in Cheah et al [8] at the angles of 90°, 135° and 180°, and the position of 1.6 D_h downstream of the bend. The numerical results as predicted by all models are in good agreement with experimental data in the upstream half of the duct. At the entrance of the bend there is a strong acceleration along the inner wall and a deceleration along the outer wall.

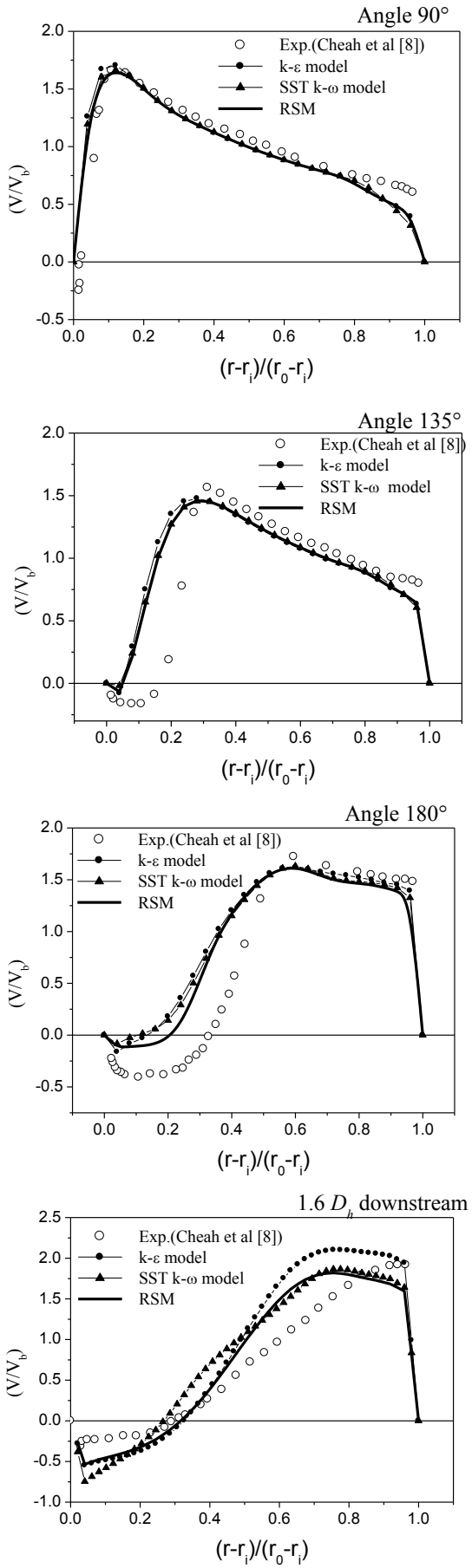

Figure 15 : Streamwise velocity profiles (1, 2, 3, 4)

The difference between predictions and experiment is greater from the angle of 135° and downstream. The predicted recirculation zone appears at a position located farter downstream than that observed in the experimental data. The numerical tool mimics correctly an acceleration of the fluid along the outer wall of the bend. It can be seen that the RSM performs better than the two other models in simulating the fluid dynamics in the second part of the flow domain as shown at the angle of 180° and at 1.6 D_h position downstream of the bend.

Figure 16 shows the pressure contours in the mid-plane of the duct. The pressure difference between the entry and the exit of the bend shows the combined linear and singular head losses. A relatively high pressure is observed on the outer wall from the angle 0° to about the angle 135°.

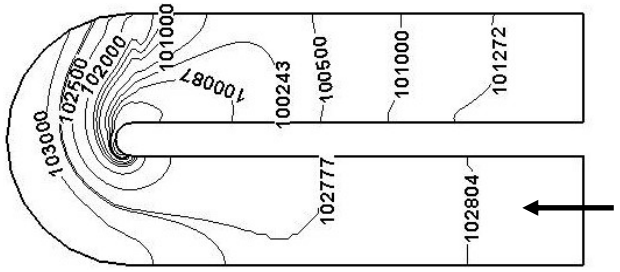

Figure 16 : Static pressure field (Pa)

This behaviour is consistent with that of the velocity field in the same area where low velocity magnitudes are observed, figure 17. Downstream of the bend, there is a low pressure region which corresponds to the region of maximum velocity. The increase in pressure observed towards the exit is explained by the fact that the kinetic energy is gradually transformed into energy of pressure. Obviously, if the duct at the exit was long enough, the linear pressure drop would be established.

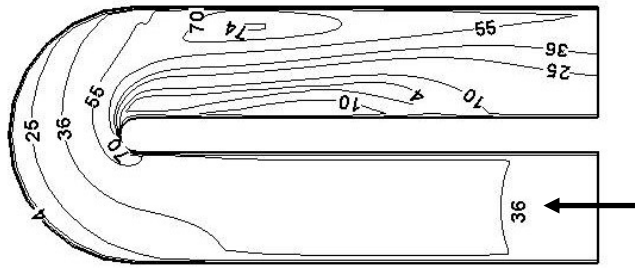

Figure 17 : Contours of velocity magnitude (m/s)

Figure 18 illustrates the streamlines on the mid-plane and at positions 0, 1, 2 and 3 D_h downstream of the bend. In the mid-plane, an important recirculation zone is seen on the inner wall, starting at a point located at the angle of about 90° and persists over a length of approximately 3 D_h. It is interesting to note that at the angle of 180° the Dean vortices are only observed in small regions close to the lateral walls. At 1 D_h downstream of the bend, three pairs of counter-rotating cells are captured. The most intense pair of cells is that located in the vicinity of the lateral walls.

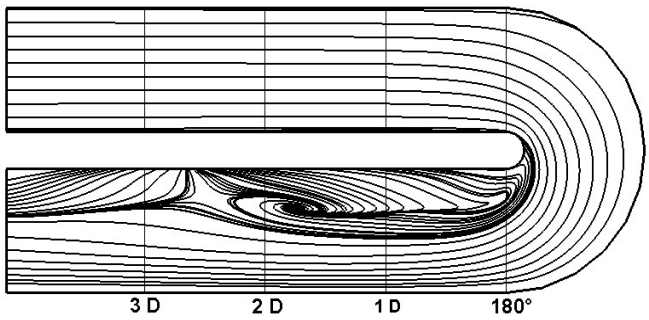

a) Mid-plane of the bend

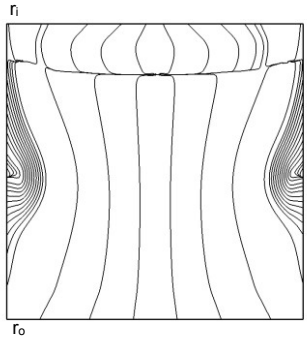

b) Angle 180°

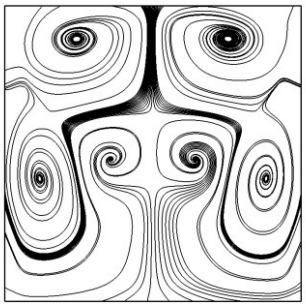

c) Position 1D_h downstream

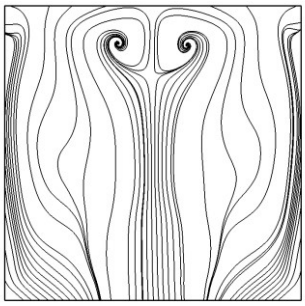

d) Position 2 D_h downstream

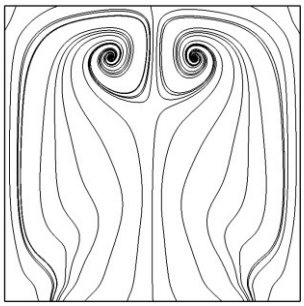

e) Position 3 D_h downstream

Figure 18 : Velocity streamlines

The two other pairs of cells, one of which is located in the centre and the other near the inner wall are relatively weak vortical structures. At the positions 2 D_h and 3 D_h only one pair of counter-rotating cells persists near the inner wall. Unexpectedly, on the right (left) hand side, the vortex motion is counter-clockwise (clockwise), inversely to that observed at the position 1 D_h.

CONCLUSION

The present study of the laminar and turbulent steady flows of a Newtonian fluid crossing 90° and 180° curved ducts of square section allowed the understanding of the phenomena which exist in such complex three-dimensional geometries. In particular, a deeper insight is provided into the development of the characteristic counter-rotating cells resulting from the radial non equilibrium between pressure and centrifugal forces within the bend. The results obtained for the two flow regimes are, overall, in agreement with the experimental data.

Moreover, very interesting phenomena are observed and the results of this study have revealed :

- The better performance of the RSM compared to the standard k-ε and the SST k-ω models in capturing the four pairs of cells in the straight duct upstream of the bend and the recirculation zone along the inner wall in the second part of the U-bend.
- The shift of the vortex core towards the inner wall as the flow advances downstream in the bend and the birth of an additional and relatively weak vortex pair located underneath the principal secondary vortex pair as obtained only by the RSM.
- A deceleration observed along the inner wall for the laminar flow. In the case of the turbulent flows the fluid accelerates then decelerates along the inner wall, the opposite phenomenon is noticed along the outer wall.
- The different behaviour of the C_f obtained by the RSM, compared to that of the two other models, is explained by the existence of the four pairs of the counter-rotating vortices.

REFERENCES

[1] Humphrey J.A.C., Taylor A.M.K., Whitelaw J.H., Laminar flow in a square duct of strong curvature. J. Fluid Mech., Vol. 83, 1977, pp. 509-527.

[2] Humphrey J.A.C., Whitelaw J.H., Yee G., Turbulent flow in a square duct with strong curvature. J. Fluid Mech., Vol. 161, 1981, pp. 371–403.

[3] Sudo K., Sumida M., Hibara H., Experimental investigation on turbulent flow in a circular sectioned 90 degree bend. Experiments in Fluids, Vol. 25, 1998, pp. 42–49.

[4] Sudo K., Sumida M., Hibara H., Experimental investigation on turbulent flow in a square sectioned 90 degree bend. Experiments in Fluids, Vol. 30, 2001, pp. 246–252.

[5] Cheng G. C., Farokhi S, On turbulent flows dominated by curvature effects. ASME J. Fluids Eng., Vol. 114, 1992, pp. 52-57.

[6] Chung Y.M., Tucker P.G., Luo K.H., Large Eddy Simulation of complex internal flows. Kluwer Academic Publishers, The Netherlands, Vol. 4, 2001, pp. 373-380.

[7] Rowe M., Measurements and computations of turbulent flow in pipe bends. J. Fluid Mech., Vol. 43, 1970, pp. 771-783.

[8] Cheah S.C., Iacovides H., Jackson D.C., Li H., Launder B.E., LDA Investigation of the flow development through rotating U ducts. ASME paper 94-GT-226, 1994.

[9] Azzola .J., Humphrey J.A.C., Developing turbulent flow in a 180° curved pipe and its downstream tangent. Report LBL-17681. Lawrence Berkeley Laboratory, University of California, 1984.

[10] Sugiyama H., Hitomi D., Numerical analysis of developing turbulent flow in a 180◦ bend tube by an algebraic Reynolds stress model. Int. J. Num. Meth. Fluids, Vol. 47, 2005, pp. 1431–1449.

[11] Kim K., Wiedner B.G., Camci C., Turbulent flow and endwall heat transfer analysis in a 90° turning duct and comparisons with measured data. Int. J. Rotating Machinery, Vol. 8(2), 2002, pp.125-140.

[12] Sudo K., Sumida M., Hibara H., Experimental investigation on turbulent flow through a circular- sectioned 180° bend. Experiments in Fluids, Vol. 28(1), 2000, pp. 51-57.

[13] Bubolz M., Wille M., Langer G., Werne U., The use of Dean vortices for cross flow microfiltration: basic principles and further investigation. Separation and Purification Technology, Vol. 26, 2002, pp. 81–89.

[14] Chung Y.M., Tucker P.G., Roychowdhury D.G., Unsteady laminar flow and convective heat transfer in a sharp 180° bend. Int. J. Heat. Fluid Flow, Vol. 24, 2002, pp. 67–76.

[15] Ramirez Duque J.L., Ramos Lucini M.A., Hydrodynamic computational evaluation in solar tubular photo-bioreactors bends with different cross sections. CT&F, Ciencia, Tecnologia y futuro, Vol. 4(4), 2011.

[16] Jones W.P., Launder B.E., The prediction of Laminarization with a Two-Equation Model of Turbulence. Int. J. Heat Mass transfer, Vol. 15, 1972, pp. 301-314.

[17] Menter F.R., Zonal Two equation k-ω Turbulence Models for Aerodynamic Flows. AIAA Paper 93-2906, 1993.

[18] Launder B.E. Reece G.J., Rodi W. Progress in the Development of a Reynolds-Stress Turbulent Closure. J. Fluid Mech., Vol. 68(3), 1975, pp. 537-566.

[19] Fluent User's Guide, Fluent Inc.

[20] Leonard B.P., A stable and accurate convective modelling procedure based on quadratic upstream interpolation. Comp. Meth. Appl. Mech.& Eng. Vol. 19, 1979, pp. 59-98.

[21] Patankar S.V., Spalding D.B., A Calculation Procedure for Heat, Mass and Momentum Transfer in Three Dimensional Parabolic Flows. Int. J. Heat Mass Transfer, Vol.15, 1972, pp. 1787-1806.